Intrinsic instabilities in premixed hydrogen flames

Intrinsic Instabilities in Premixed Hydrogen Flames: Parametric Variation of Pressure, Equivalence Ratio, and Temperature. Part 1 - Dispersion Relations in the Linear Regime

Lukas Berger[a,*], Antonio Attili[b], Heinz Pitsch[a]

[a] *Institute for Combustion Technology, RWTH Aachen University, 52056 Aachen, Germany*
[b] *Institute for Multiscale Thermofluids, School of Engineering, University of Edinburgh, Edinburgh, EH9 3FD, United Kingdom*

Abstract

The impact of intrinsic combustion instabilities is studied for lean premixed hydrogen flames by means of a series of simulations at different equivalence ratios [0.4-1.0], unburned temperatures [298K-700K], and pressures [1bar-20bar]. In addition to the Darrieus-Landau, or hydrodynamic, instability, lean premixed hydrogen flames are prone to thermodiffusive instabilities, which lead to significant flame front wrinkling and a chaotic process of formation and destruction of cellular structures along the flame front. Theoretical models are not yet capable of accurately describing the evolution of such flames, so the propensity of lean hydrogen flames to develop instabilities is studied numerically in a parametric variation in this work. A stability analysis is conducted, in which planar flames are initially exposed to weak harmonic perturbations and the response of the flame is studied. In the initial phase referred to as linear phase, a growth or decrease of the initially imposed perturbation amplitude is observed, while for long times, chaotic cellular structures are formed along the flame front, which are studied in part 2 of this work (L.Berger et al., Combust. Flame, 2021). The growth rates of the perturbation amplitude that are obtained from the initial phase are a measure of the strength of the intrinsic instability mechanisms and vary with respect to the wave number of the harmonic perturbation yielding characteristic dispersion relations. A decrease of equivalence ratio and unburned temperature and an increase of pressure are found to enhance the growth rates and hence intrinsic instabilities. The variation of dispersion relations is analyzed with respect to variations of the expansion ratio, the effective Lewis number of the mixture, and the Zeldovich number. For the lean hydrogen flames, with increasing pressure a decrease of the cut-off wave number, which represents the change of the sign of the dispersion relation at high wave numbers, is observed. This is the opposite trend compared to flames that are not affected by thermodiffusive instabilities. Further, numerical growth rates are compared to theoretical models. The results show that lean hydrogen flames are prone to develop instabilities at conditions that are relevant to several combustion devices such as gas turbines that operate at lean equivalence ratios, elevated pressures and temperatures or domestic and industrial heaters that operate at low temperatures and ambient pressure.

Keywords: Thermodiffusive Instability, DNS, Hydrogen, Premixed, Preferential Diffusion

1. Introduction

The recent rise of electricity production from renewable energy sources has increased the need for appropriate energy storage, thus promoting the use of hydrogen as a carbon-free energy carrier [1]. One possibility to integrate hydrogen into the existing energy infrastructure is its thermochemical energy conversion [2]. However, a variety of challenges and opportunities arises for combustion processes that involve hydrogen as a fuel. In particular, lean hydrogen/air flames are prone to combustion instabilities, which can substantially change flame dynamics, heat release rates, and flame speed. These aspects are highly relevant for safety considerations in any combustion device, e.g., to avoid flame flash back, but can be also exploited to increase thermal efficiencies [3].

In lean premixed hydrogen flames, combustion instabilities originate from the low Lewis number of molecular hydrogen, which induces strong differential diffusion effects within the flame front. The low Lewis number of hydrogen results from the high molecular diffusion of hydrogen compared to the thermal diffusivity of the mixture. The disparity of the heat and hydrogen mass fluxes leads to an amplification of small flame front perturbations such that strongly wrinkled flame fronts are observed leading to significantly enhanced fuel conversion rates. This instability mechanism is known as the thermodiffusive instability. Additionally, the flame propagation is affected by the hydrodynamic instability mechanism, which arises from the density jump across the flame front, and exists for any premixed flame irrespective of the Lewis number.

Extensive theoretical analyses of such instabilities and their impact on the stability of planar flames have been conducted, but yet, none of the theoretical models is capable of accurately describing the flame evolution of lean premixed hydrogen. The theoretical studies by Clavin and Williams [4] and Matalon and Matkowsky [5] assumed a global one-step reaction with large activation energy. In this model, all reactions are assumed to

*Corresponding author
Email address: l.berger@itv.rwth-aachen.de (Lukas Berger)

occur in a thin region compared to the preheat zone and the flame sheet iso-surface is located close to the burned gases. The model formulation was extended by Giannakopoulos et al. [6] and Clavin and Graña-Otero [7] by considering different iso-surfaces within the flame such that the effect of flame curvature, strain rate, and stretch on the flame speed is determined for different choices of iso-surfaces. However, in these analyses [4–7], the flame stretch rate, curvature, and strain rate are assumed to be small compared to the flame time and flame thickness and the mixture's effective Lewis number is assumed to be close to unity. In contrast, the analyses of Sivashinsky [8, 9] allow for large values of the stretch rate and for Lewis numbers sufficiently smaller than unity as it is the case for lean premixed hydrogen flames, but assume the density jump throughout the flame front to be small. For these conditions, an integro-differential equation is derived that predicts the evolution of a corrugated flame front and can qualitatively reproduce the formation of cellular structures along the flame front that are typical features of thermodiffusively unstable flames.

Theoretical models are presently not capable of accurately describing the evolution of lean premixed hydrogen flames, as either Lewis numbers close to unity are assumed, whereas the Lewis number of hydrogen is significantly lower than unity, or small variations of density are assumed, while significant density variations are observed in actual flames. Attili et al. [10] showed that even for methane/air flames, whose Lewis number is close to unity and which do not feature thermodiffusive instabilities, the theoretical models are missing certain trends and lack an accurate description. Thus, since thermodiffusive instabilities can significantly affect the flame evolution, a comprehensive quantification of intrinsic instabilities in lean hydrogen/air flames is necessary. For instance, Berger et al. [11] showed that thermodiffusive instabilities can lead to four times higher consumption speeds in lean hydrogen/air mixtures at ambient conditions. For this, a series of high-fidelity simulations that employ a detailed chemical mechanism to avoid assumptions related to the reduction of chemical mechanisms and resolve all length and time scales, such as spatial gradients and the characteristic time scales of chemical reactions, has been performed. A rigorous assessment of the strength of the intrinsic instability mechanisms can be pursued by means of a a stability analysis, in which a planar flame is initially exposed to a weak harmonic perturbation and the response of the flame is studied. In the initial phase referred to as linear phase, an exponential growth or decrease of the initially imposed amplitude of the perturbation is observed and measuring the respective growth rates with respect to the wave length of the initial perturbation yields a dispersion relation. Studying such dispersion relations at different conditions allows for a rigorous assessment of the impact of the instability mechanisms.

Frouzakis et al. [12] numerically investigated dispersion relations of hydrogen/air flames at different equivalence ratios of $0.5 < \phi < 2.0$ at atmospheric conditions using a detailed chemical mechanism. While good agreement among the numerical and theoretically predicted dispersion relations is seen for the cases with $\phi \geq 0.75$, large discrepancies are observed for the leaner case, where the thermodiffusive mechanism becomes dominant. Similar findings are observed by Altantzis et al. [13], who studied a lean hydrogen/air flame at $\phi = 0.6$ at 5bar and an unburned temperature of 298K using a single-step global reaction. As expected for lean conditions, the model of Matalon et al. [14] does not capture the inflection point at small wave numbers and no stabilization at high wave numbers occurs. The model by Sivashinsky [9] leads to a significant underprediction as the variation of densities is neglected. Further numerical studies on dispersion relations have been performed by Kadowaki et al. [15], Yuan et al. [16], Sharpe [17], and Denet et al. [18], who all used a one-step global reaction and controlled the conditions of the flame by global flame parameters, such as the Zeldovich number, the expansion ratio, and the Lewis number, instead of choosing a specific fuel for their parametric variations. An increase of the expansion ratio or a reduction of the Lewis number are shown to increase growth rates and also lead to an increase of the cut-off wave number, which represents the wave number when the dispersion relation changes sign at high wave numbers. A similar observation regarding the cut-off wave number is reported by Attili et al. [10], who numerically investigated dispersion relations of lean methane/air flames at different pressures using detailed chemistry. They demonstrated that an increase of pressure leads to an increase of the cut-off wave number even for unity Lewis number flames; a trend that is not observed in theoretical models, which predict a pressure independent value.

While several studies have numerically investigated dispersion relations by means of global flame parameters, such as the expansion ratio and the Lewis number, dispersion relations of real fuels have been only studied for selected conditions. In particular, a comprehensive study of lean hydrogen/air flames that provides quantitative growth rates in a large parametric space while using realistic transport models including for instance the Soret effect, which was shown to be important in hydrogen flames [19, 20], is yet missing, but is required to quantitatively assess at which conditions the effects of thermodiffusive instabilities have a leading order effect or may be negligibly small. Further, such data can be used in various kinds of models, e.g. to estimate the relevant region of intrinsic instabilities in the turbulent combustion regime diagram, for which the characteristic turbulent time scales are compared with the time scales of the intrinsic instabilities. The latter are typically estimated by theoretical models [21] due to the lack of data, but could be replaced by the data obtained in this work.

Thus, in the first part of this work, dispersion relations of lean hydrogen/air flames are computed at various conditions for a large parametric space of equivalence ratios, unburned temperatures, and pressures. The variation of growth rates with different conditions is analyzed and linked to a change of the intrinsic flame parameters such as the expansion ratio, the Lewis number, or the Zeldovich number and a comprehensive comparison with theoretical models is provided. The flame behavior for long times, which is referred to as non-linear phase and features the formation of chaotic cellular structures along the flame front, is studied in part 2 of this work [22]. The manuscript is structured as follows: First, theoretical models to predict dispersion relations are discussed. Thereafter, the numerical con-

figuration, the governing equations, and the conditions of the parametric variation are introduced. Then, the analysis of the numerically obtained dispersion relations are presented and discussed.

2. Theoretical Background

Planar flames that are exposed to an initial weak harmonic perturbation will react to such disturbances and lead to an increase or decrease of the amplitude of the initial perturbation. Further, the flame's response is found to depend on the wave number of the initial perturbation as typically, small wave numbers are destabilizing due to the hydrodynamic instability while a stabilization is observed for large wave numbers due to the thermodiffusive processes within the flame front. If the harmonic perturbation of a planar flame front is sufficiently weak, an exponentially increasing or decreasing amplitude can be observed. The dependence of the exponential growth rate ω on the wavelength k of the perturbation is referred to as dispersion relation. The initial phase, during which an exponential growth rate is observed, will be referred to as linear phase. This phase is terminated by the transition to the non-linear phase, when the shape of the perturbed flame does not follow a harmonic signal anymore.

Dispersion relations represent an efficient way to study the impact of instabilities at different conditions and the analysis of such flames does not introduce additional assumptions as the determination of growth rates is well defined. Furthermore, the dispersion relations can be directly compared to theoretical predictions as these flames are only weakly stretched, which is a typical assumption in theoretical derivations. As this work also provides a comparison with theoretical predictions, the relevant theoretical models are presented in the following.

If the mixture's Lewis number is sufficiently close to unity, Matalon et al. [14] derived a dispersion relation of the following form

$$\overline{\omega} = \omega_{\mathrm{DL}}\overline{k} - \delta[B_1 + \beta(Le_{\mathrm{eff}} - 1)B_2 + PrB_3]\overline{k}^2, \tag{1}$$

where the growth rate $\overline{\omega} = \omega\tau_{\mathrm{F}}$ and wave number $\overline{k} = kl_{\mathrm{F}}$ are non-dimensional variables that are normalized by the flame time τ_{F} and the flame thickness l_{F}. The thermal flame thickness l_{F} is defined by the maximum gradient criterion in a one-dimensional unstretched flame as

$$l_{\mathrm{F}} = \frac{T_{\mathrm{b}} - T_{\mathrm{u}}}{\max(\nabla T)}, \tag{2}$$

where T_{u} and T_{b} are the unburned and adiabatic flame temperature, respectively. The flame time is defined as

$$\tau_{\mathrm{F}} = l_{\mathrm{F}}/s_{\mathrm{L}}, \tag{3}$$

where s_{L} is the laminar burning velocity of an unstretched flame. In Eq. 1, the term ω_{DL} refers to the linear growth rate resulting from the hydrodynamic instability mechanism, and $\delta = l_{\mathrm{D}}/l_{\mathrm{F}}$ is the ratio between the thermal flame thickness l_{F} and the diffusive flame thickness $l_{\mathrm{D}} = D_{\mathrm{th}}/s_{\mathrm{L}}$, which is defined by the thermal diffusivity D_{th} and the laminar unstretched burning velocity s_{L}. Note that δ is defined analogously to Altantzis et al. [13], who also normalized the wave number by the thermal flame thickness, while Matalon et al. [14] used a different normalization, which requires a different definition of δ. Le_{eff} is the effective Lewis number of the two reactants, β is the Zeldovich number, and Pr is the Prandl number. The coefficients B_1, B_2, and B_3 depend on the variation of the transport coefficients such as the conductivity with respect to temperature and the expansion ratio and their definitions are provided in the supplementary material. It is worth noting that the coefficients B_1, B_2, and B_3 are always positive and $B_1 \geq 1$, $B_2 \geq 1/2$, and $B_3 \geq 0$. The expansion ratio σ is defined by the unburned and burned density, ρ_{u} and ρ_{b}, respectively, as

$$\sigma = \frac{\rho_{\mathrm{u}}}{\rho_{\mathrm{b}}}. \tag{4}$$

The Zeldovich number β is given by

$$\beta = \frac{E}{R}\frac{(T_{\mathrm{b}} - T_{\mathrm{u}})}{T_{\mathrm{b}}^2}, \tag{5}$$

where R is the universal gas constant, T_{b} is the adiabatic flame temperature, and E is the activation energy that can be determined from [23]

$$\frac{E}{R} = -2\frac{\mathrm{d}(\rho_{\mathrm{u}} s_{\mathrm{L}})}{\mathrm{d}(1/T_{\mathrm{b}})}. \tag{6}$$

Following Sun et al. [24], the derivative in Eq. 6 is evaluated from two one-dimensional flamelets by diluting the mixture with a tiny amount of nitrogen ($\Delta Y_{\mathrm{N_2}} \approx \pm 0.3\%$) while keeping equivalence ratio, pressure, and unburned temperature the same. According to Joulin et al. [25], the effective Lewis number Le_{eff} is defined as a weighted sum of the Lewis number of the excess reactant Le_{E} and the Lewis number of the deficient reactant Le_{D} yielding

$$Le_{\mathrm{eff}} = 1 + \frac{(Le_{\mathrm{E}} - 1) + (Le_{\mathrm{D}} - 1)\mathcal{A}}{1 + \mathcal{A}}, \tag{7}$$

where, for lean mixtures, the factor $\mathcal{A}$ is given by

$$\mathcal{A} = 1 + (\phi^{-1} - 1)\cdot\beta \tag{8}$$

and ϕ is the equivalence ratio. Eq. 8 is obtained if unity reaction orders are assumed, but no significant effect is observed for the conditions of this study if choosing non-unity reaction orders as discussed in the supplementary material.

The term related to the hydrodynamic instability is destabilizing for any wave number ($\omega_{\mathrm{DL}} \geq 0$). According to Landau [26] and Darrieus [27], its growth rate can be expressed as

$$\omega_{\mathrm{DL}} = \frac{\sqrt{\sigma^3 + \sigma^2 - \sigma} - \sigma}{\sigma + 1} \tag{9}$$

and only depends on the expansion ratio σ. The second term appearing in Eq. 1 describes the effect of the thermal-diffusive processes and is often negative and hence stabilizing. However, for a sufficiently small effective Lewis number as for lean premixed hydrogen flames, this term becomes positive and the series expansion should be carried out to higher terms of the wave number $\overline{k}$ to include a stabilizing term.

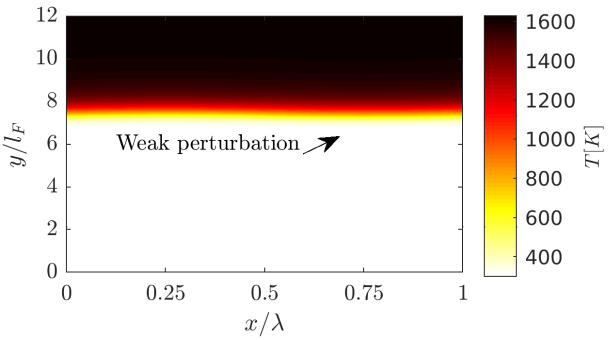

Figure 1: Case 'Ref': Snapshot of the initial temperature field. Unburned mixture is entering the domain at the bottom while burned gases leave the domain at the top. The configuration is periodic in lateral direction and the flame front is perturbed with a small sinusoidal perturbation with wave length $\lambda = 24 l_F$. Coordinates in y-direction are normalized by l_F and coordinates in x-direction are normalized by λ.

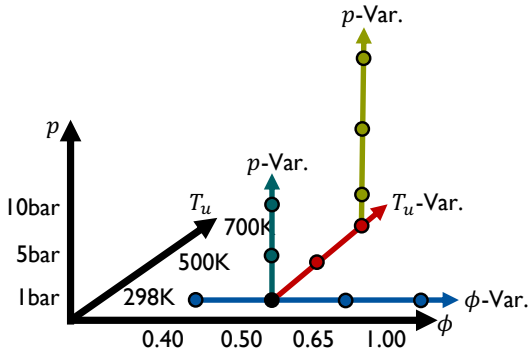

Figure 2: Visualization of the parametric variation of equivalence ratio, unburned temperature, and pressure.

Sivashinsky [8, 9] derived a dispersion relation that allows for Lewis numbers sufficiently smaller than unity as it is the case for lean premixed hydrogen flames, but assumes the density jump within the flame front and hence, the expansion ratio to be small. Sivashinsky [8] derived the following implicit dispersion relation

$$0 = \frac{(Le - q)(p - r)}{Le - q + p - 1} - \frac{\beta}{2}, \tag{10}$$

where the terms q, p, r are given as follows

$$p = \frac{1}{2}\left[1 + \sqrt{1 + 4(\delta\overline{\omega} + \delta^2\overline{k}^2)}\right], \tag{11}$$

$$q = \frac{Le}{2}\left[1 + \sqrt{1 + \frac{4(\delta\overline{\omega}Le + \delta^2\overline{k}^2)}{Le^2}}\right], \tag{12}$$

$$r = \frac{1}{2}\left[1 - \sqrt{1 + 4(\delta\overline{\omega} + \delta^2\overline{k}^2)}\right]. \tag{13}$$

Following Sivashinsky [28], for Lewis numbers close to the critical Lewis number, Eq. 10 yields

$$\overline{\omega} = \delta\left[\frac{\beta}{2}(1 - Le) - 1\right]\overline{k}^2 - 4\delta^3\overline{k}^4. \tag{14}$$

It is worth noting that in the limit $\sigma = 1$, Eq. 1 derived by Matalon et al. [14] becomes identical to Eq. 14 as $B_1 \to 1$, $B_2 \to 1/2$, and $B_3 \to 0$ if $\sigma \to 1$, but Eq. 14 additionally contains a fourth order term that is stabilizing irrespective of the mixture's effective Lewis number.

3. Configuration and Numerical Methods

3.1. Configuration

The simulations for the analysis of the linear regime are conducted in two-dimensional rectangular domains as shown in Fig. 1, where the lateral size of the domain L_x is selected to be equal to the wave length $\lambda = 2\pi/k$ of the harmonic perturbation. Periodic boundary conditions are applied in lateral direction x and, in streamwise direction denoted by y, an inflow at the bottom of the domain and an outlet at the top of the domain are prescribed. At the inlet, unburned mixture with a velocity equal to the laminar unstretched burning velocity enters the domain while the burned gases downstream of the flame leave the domain at the outlet, c.f. Fig. 1. The domain length in the streamwise direction is chosen sufficiently large, i.e. $L_y = 12 l_F$ such that all species and temperature profiles possess zero gradients at the boundary conditions. The simulation is initialized by a one-dimensional unstretched flamelet that is aligned in y-direction and is obtained from a FlameMaster [29] calculation. The flame front is then perturbed with a weak harmonic perturbation $F(x)$ of the form

$$F(x) = A_0 \cdot \cos(kx), \tag{15}$$

where A_0 is the perturbation's amplitude. In particular, the initial solution is obtained by mapping one-dimensional flamelets into the simulation domain and shifting them in y-direction according to the imposed perturbation.

Tab. 1 summarizes all simulations that have been performed. As a reference case, the conditions of the unburned mixture are set to an equivalence ratio of $\phi = 0.5$, an unburned temperature $T_u = 298$K, and a pressure of $p = 1$bar. Parametric variations are conducted with respect to equivalence ratio, unburned temperature, and pressure while the other parameters are kept constant. In addition to these three variations, a fourth variation of pressure at $\phi = 0.5$ and $T_u = 700$K has been performed to include high pressure, high temperature conditions that represent characteristic conditions for gas turbine applications [30]. A visualization of the four different parametric variations is shown in Fig. 2. Tab. 1 lists the burning velocity s_L and the thermal flame thickness l_F of a one-dimensional laminar unstretched flame, the flame's expansion ratio σ, the Zeldovich number β, and the effective Lewis number Le_{eff} for each case.

3.2. Governing Equations and Numerical Methods

The flow is modeled by the reacting Navier-Stokes equations in the low-Mach limit [31]. The fluid is assumed to be an ideal gas and chemical reactions are modeled by the mechanism of Burke et al. [32] that contains 9 species and 46 reactions. The viscosity of the mixture is determined by the formula according to Wilke [33] and the species viscosities are determined according to kinetic theory [34]. The thermal conductivity of the

Table 1: Overview of the performed simulations. For each case, the equivalence ratio ϕ, the pressure p, the unburned temperature T_u, the laminar unstretched burning velocity s_L, the flame thickness l_F, the expansion ratio σ, the Zeldovich number β, and the effective Lewis number Le_{eff} are given.

Case name	ϕ	p [bar]	T_u [K]	s_L [cm/s]	l_F [μm]	τ_F [ms]	σ	β	Le_{eff}
Reference case:									
Ref	0.5	1	298	45.2	438	0.97	5.04	9.2	0.37
Variation of equivalence ratio:									
Eq040	0.4	1	298	17.4	714	4.35	4.44	11.4	0.34
Eq065	0.65	1	298	99.8	363	0.36	5.79	7.4	0.43
Eq100	1.0	1	298	228.9	372	0.16	6.84	6.4	0.68
Variation of unburned temperature:									
Tu500	0.5	1	500	179.6	441	0.25	3.31	8.5	0.39
Tu700	0.5	1	700	523.2	533	0.10	2.57	3.8	0.44
Variation of pressure:									
p05	0.5	5	298	21.5	119	0.55	5.04	12.6	0.35
p10	0.5	10	298	12.0	92	0.76	5.04	16.5	0.34
Variation of pressure at T_u = 700K:									
Tu700p03	0.5	3	700	395.0	128	0.033	2.58	5.5	0.41
Tu700p10	0.5	10	700	216.8	33	0.015	2.58	7.5	0.38
Tu700p20	0.5	20	700	132.9	18	0.014	2.59	8.9	0.37

species are computed according to Eucken [35] and the thermal conductivity of the mixture is evaluated as suggested by Mathur et al. [36]. The species diffusivities D_i are determined from the thermal conductivity λ, the density ρ, and the specific heat capacity c_p as $D_i = \lambda/(\rho c_p \mathrm{Le}_i)$ by imposing spatially homogeneous Lewis numbers. The Lewis numbers were taken from the burned gas region of one-dimensional unstretched premixed flames, which was found to yield the best approximation for the unstretched laminar burning velocity. A table of relevant Lewis numbers for the different cases is provided in the supplementary material. Following Zhou et al. [19] and Schlup et al. [20], molecular diffusion due to the Soret effect is also included and a summary of the model is provided by Schlup et al. [37]. For the species diffusion velocity appearing in the species and temperature equations, a velocity-correction approach [38] is applied to enforce mass conservation.

A semi-implicit finite difference code, based on the Crank-Nicolson time advancement scheme, and an iterative predictor corrector scheme is employed [39]. Spatial and temporal staggering is used to increase accuracy and stability. The Poisson equation for the pressure is solved by the multi-grid HYPRE solver [40]. Momentum equations are discretized with a second order scheme. In the species and temperature equations, the convective term is discretized with a third order WENO scheme [41] and the diffusion operator is discretized with second order central differences. The temperature and species equations are advanced by utilizing Strang's operator splitting [42]. The time integration of the chemical source terms employs a time-implicit backward difference method, as implemented in the stiff ODE solver CVODE as part of the SUNDIALS suite [43]. The initial amplitude of the harmonic perturbation $A_0 = A(t = 0)$ is set to $A_0 = 0.04 l_F$ requiring meshes with a resolution of $\Delta x = 0.01 l_F$. It is worth noting that the high mesh resolution of these simulations is only required to adequately resolve the flame perturbation as the laminar flame speed, heat release, temperature, and species profiles of a one-dimensional premixed unstretched flame computed by FlameMaster [29] are already adequately recovered with ten to fifteen grid points per flame thickness.

4. Results and Discussion

4.1. Determination of Dispersion Relations from Numerical Simulations

Fig. 3 shows different iso-lines of temperature at different time instances (solid lines) for case 'Ref' with an initial perturbation of $\lambda = 4 l_F$. Furthermore, a harmonic signal is fit to the iso-surfaces (dashed lines) in Fig. 3. The amplitude of the perturbation is seen to grow in time while the shape of the flame front initially follows the harmonic signal but increasingly starts deviating from a harmonic signal for later times. The amplitude $A(t)$ of the flame iso-lines is measured in time and the exponential growth rate ω is determined as

$$\omega = \frac{\mathrm{d}\ln(A(t))}{\mathrm{d}t}. \tag{16}$$

If the amplitude follows an exponential growth $A(t) = \exp(\omega t)$, a constant growth rate ω is obtained. Fig. 4 shows that, after an initial transient, the growth rate ω levels off at a constant value indicating an exponential growth while for later times, ω starts deviating from the constant value as the flame evolution enters the non-linear phase. The deviation from the constant value in Fig. 4 is consistent with the deviation of the iso-surfaces from the harmonic shape in Fig. 3. The constant value corresponds to

the growth rate of the linear phase. Note that a negative value indicates a reduction of the amplitude of the initial perturbation. Measuring these growth rates for different values of the perturbation wave length λ, yields the dispersion relation.

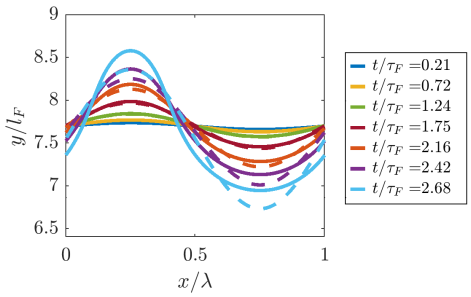

Figure 3: Case 'Ref': Visualization of the increase of the initial perturbation with $\lambda = 4l_F$ by means of iso-surfaces of temperature at different time instances. Coordinates in y-direction are normalized by l_F and coordinates in x-direction are normalized by λ.

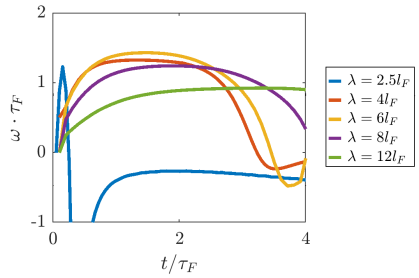

Figure 4: Case 'Ref': Growth rate ω of the exponentially growing amplitude $A(t)$ for different perturbation wave lengths λ. Growth rates and time are normalized by the flame time τ_F.

4.2. Discussion of Numerical Dispersion Relations

Fig. 5 shows the numerical dispersion relations for different values of the equivalence ratio, the unburned temperature, the pressure at low unburned temperatures, and the pressure at elevated unburned temperatures. Symbols refer to simulations, from which growth rates are determined numerically, and to improve the visualization, a spline is fitted to the data points (solid lines). Fig. 5 also contains the growth rates ω_{DL} of the hydrodynamic instability mechanism from Eq. 9 (dashed lines). It is worth noting that additional simulations have been performed at even larger wave numbers at $\bar{k} \approx \pi$, which are not shown in Fig. 5 due to their large negative growth rate values.

All dispersion relations reveal positive growth rates for a wide range of wave numbers. The cut-off wave length $\lambda_c = 2\pi/k_c$, for which the growth rate changes sign, is in the range of $2.3l_F < \lambda_c < 3.0l_F$ and the wave length of the maximum growth rate is found to be between $4.5l_F < \lambda_{\omega_{max}} < 5.6l_F$. Certain cases, e.g. case 'Ref', possess growth rates that exceed the growth rate associated with the hydrodynamic instability ω_{DL} indicating a positive contribution of the thermodiffusive instability mechanism for small wave numbers while for other

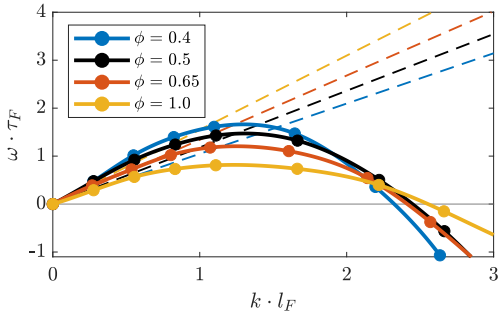

(a) ϕ-Variation at p = 1 bar and T_u = 298 K

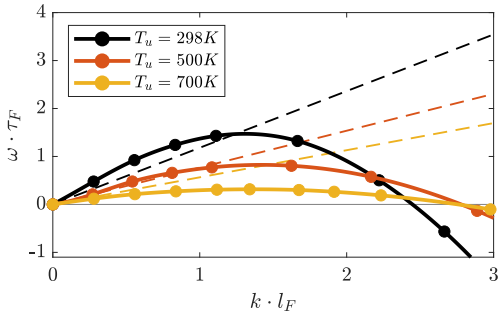

(b) T_u-Variation at ϕ = 0.5 and p = 1 bar

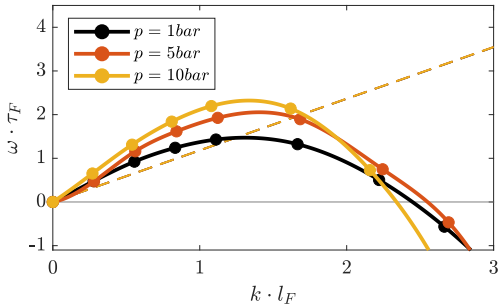

(c) p-Variation at ϕ = 0.5 and T_u = 298 K

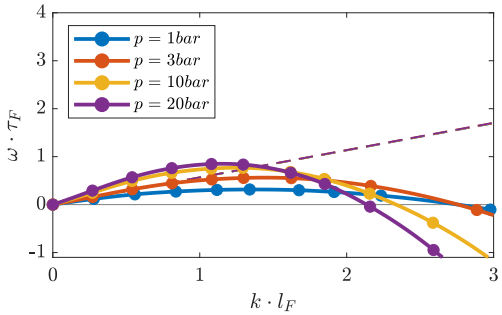

(d) p-Variation at ϕ = 0.5 and T_u = 700 K

Figure 5: Dispersion relations for variations of ϕ, T_u, and p. Black lines and symbols refer to the reference case 'Ref' (ϕ = 0.5, T_u = 298 K, p = 1 bar). Symbols refer to the growth rates extracted from simulations, solid lines represent cubic spline fits to these growth rates, and dashed lines are the growth rates associated with the hydrodynamic instability, cf. Eq. 9. For each case, growth rates and wave numbers are normalized by the flame time τ_F and flame thickness l_F of the corresponding unstretched one-dimensional flamelet.

cases such as case 'Tu700', the numerical growth rates are always below the growth rates related to the hydrodynamic in-

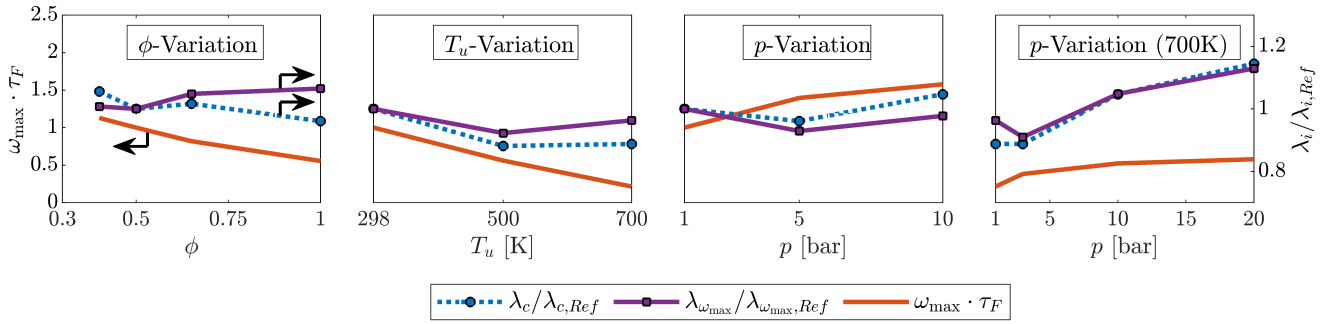

Figure 6: Variation of the peak growth rate $\omega_{\max}$, the wave length of the peak $\lambda_{\omega_{\max}}$, and the cut-off wave length λ_c with respect to the four different parametric variations of equivalence ratio ϕ, unburned temperature T_u, pressure p, and pressure at elevated unburned temperatures $p(700K)$. Both wave lengths are normalized by the values of case 'Ref' that are $\lambda_{c,\mathrm{Ref}} = 2.6 l_F$ and $\lambda_{\omega_{\max},\mathrm{Ref}} = 4.8 l_F$.

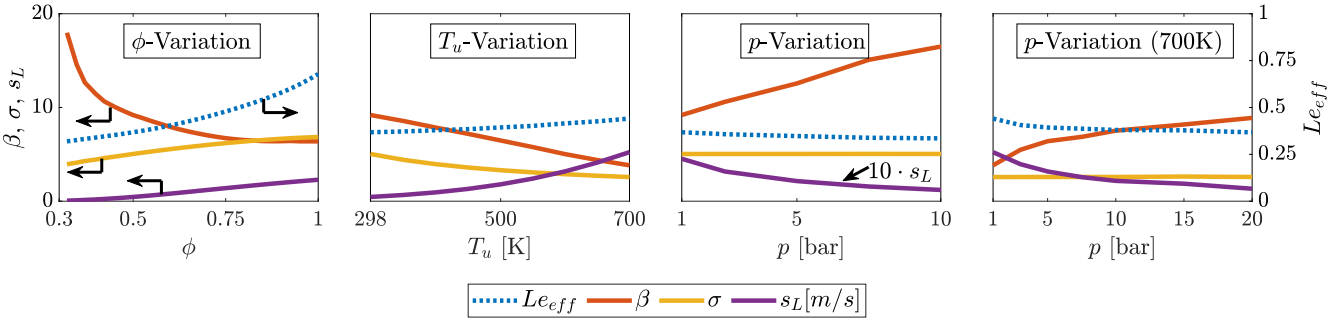

Figure 7: Variation of the expansion ratio σ, the Zeldovich number β, the effective Lewis number Le_{eff}, and the laminar unstretched burning velocity s_L with respect to the four different parametric variations of equivalence ratio ϕ, unburned temperature T_u, pressure p, and pressure at elevated unburned temperatures $p(700K)$.

stability mechanism indicating that the thermodiffusive mechanism has a negative contribution to the growth rates of the dispersion relation at any wave number. Generally, the measured dispersion relations allow to quantify the level of instability and therefore, cases with high peak growth rates will be considered as more unstable than cases with small peak growth rates. It is worth noting that a variation of pressure does not change the expansion ratio of the flames such that the growth rates of the hydrodynamic instability remain unaffected, so only one single dashed line is displayed for the pressure variations. Further, note that for $k \to 0$, the numerical dispersion relations are expected to coincide with the dashed line of the hydrodynamic instability, so further simulations would be required to properly explore this limit, which is outside the scope of this work.

Fig. 6 highlights the variation of the peak growth rates with respect to equivalence ratio, unburned temperature, and pressure. A decrease of equivalence ratio and unburned temperature and an increase of pressure are found to enhance intrinsic instabilities. It is worth stressing the propensity of intrinsic instabilities to increase with rising pressure as many combustion devices operate at elevated pressures. Furthermore, Fig. 6 shows the cut-off wave length λ_c and the wave length of the peak growth rate $\lambda_{\omega_{\max}}$, which are normalized by the value of case 'Ref'. Both wave lengths are only weakly affected by the parametric variation and it is worth noting that the determination of $\lambda_{\omega_{\max}}$ is subject to a relative error of about 13-21% (if allowing an error of 1% for the determination of the peak growth rate) for all cases. Hence, the peculiar reduction of $\lambda_{\omega_{\max}}$ for case 'Tu700p03' occurs within the estimated uncertainties. However, uncertainties for λ_c are significantly lower (< 1% for all cases if allowing for the same amount of error, namely an error of 1% of the peak growth rate, for the determination of the growth rate, where the dispersion relation changes sign) and generally, a weak tendency of an increasing cut-off wave λ_c length towards unstable conditions is observed, most prominently visible during the increase of pressure at elevated temperatures. This is interesting if compared to the study of Attili et al. [10], who reported the opposite trend for lean methane/air mixtures, namely a decrease of λ_c for increasing pressure. This difference is discussed in detail in the remainder of this paper.

In the following, the correlation between the variation of the numerical dispersion relations, in particular their peak growth rates, and the flame parameters σ, β, and Le_{eff} is discussed. Fig. 7 shows the variation of σ, β, and Le_{eff} with respect to the four different parametric variations. The variation of pressure only affects the Zeldovich number β while the expansion ratio σ and the effective Lewis number Le_{eff} remain constant, so the increased peak growth rates can be linked to an increase of β for the pressure variation. However, the effect of σ and Le_{eff} on the growth rates cannot be isolated as the variations of unburned temperature and equivalence ratio affect at least two of the three parameters σ, β, and Le_{eff}. For this reason, a power law fit of the peak growth rates $\omega_{\max}$ with respect to σ, β, and Le_{eff} is

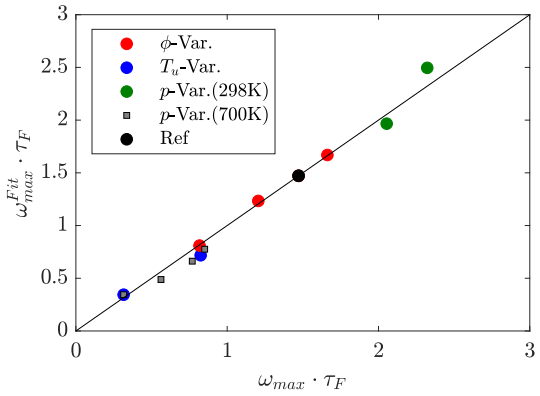

Figure 8: Comparison of numerically measured peak growth rates (abscissa) versus growth rates predicted by Eq. 17 (ordinate). Each symbol represent one case of Tab. 1 and case 'Ref' is marked by a black symbol.

considered,

$$\overline{\omega}_{\max} = \overline{\omega}_{\max,\mathrm{Ref}} \cdot \left(\frac{\sigma}{\sigma_{\mathrm{Ref}}}\right)^{\alpha_\sigma} \left(\frac{\beta}{\beta_{\mathrm{Ref}}}\right)^{\alpha_\beta} \left(\frac{Le_{\mathrm{eff}}}{Le_{\mathrm{eff,Ref}}}\right)^{\alpha_{Le_{\mathrm{eff}}}}, \qquad (17)$$

to assess the impact of each parameter on $\omega_{\max}$. It is important to stress that Eq. 17 is not derived from first principles, but represents a simple fit as one way among other possible options to efficiently disentangle the effect of the different parameters on the peak growth rates. Similar power law fits have been already suggested, e.g. to assess the critical radius, which characterizes the onset of intrinsic instabilities in spherically expanding flames [44], to assess the variability of the cut-off wave length with pressure [10], or generally, for flame parameters such as the laminar burning velocity [45]. In the following, the suitability of assessing $\overline{\omega}_{\max}$ by Eq. 17 is discussed. For this, the three scaling coefficients α_{i} are fitted to the values of $\sigma, \beta, Le_{\mathrm{eff}}$, and $\omega_{\max}$ of the different cases and the values of case 'Ref' are taken as reference values. The data from cases 'Tu700p03', 'Tu700p10', and 'Tu700p20' are not used to fit the coefficients α_{i} but used for an assessment of the quality of the fit.

Fig. 8 shows a comparison of the peak growth rates $\omega_{\max}$ from the simulations and the values predicted by Eq. 17. It is worth noting that case 'Tu700' is displayed twice (blue dot that contains a grey box) as it belongs to the parametric variations of unburned temperature and pressure at elevated temperatures. Good agreement among the actual and predicted values is observed. Even for the parametric variation of pressure at elevated unburned temperatures that has not been used for the fit, good agreement is achieved indicating a constant value of α_β for different conditions. The least square fit yields the following values for the exponents

$$\alpha_\sigma = 0.93, \quad \alpha_\beta = 0.73, \quad \alpha_{Le_{\mathrm{eff}}} = -1.03. \qquad (18)$$

It is worth noting that in Eq. 17, case 'Ref' has been used for scaling the growth rates and flame parameters. While choosing a different case or using instead a power law with a fitted constant of proportionality that replaces the coefficients labeled by the index 'Ref' could affect the values of the exponents α_{i}, it is shown in the supplementary material that such variations do not significant affect the determination of the exponents α_{i}. Thus, an increase of Zeldovich number β and expansion ratio σ enhances the peak growth rates and an increase of Lewis number decreases the peak growth rates. Hence, the steep increase of the Zeldovich number and the reduction of the effective Lewis number for decreasing equivalence ratios compensate the reduction of the expansion ratio yielding an increase of peak growth rates. It is worth noting that in addition to the power law proposed in Eq. 17, a similar power law using the term $(1 - Le_{\mathrm{eff}})$ instead of Le_{eff} for scaling, which is motivated by the theoretical formulas of Matalon [14] and Sivashinsky [9], has been tested yielding almost identical predictions of $\omega_{\max}$ and values of α_{i} just that $\alpha_{Le_{\mathrm{eff}}} \approx -\alpha_{(1-Le_{\mathrm{eff}})}$. Thus, consistently, an increase of Lewis number decreases the peak growth rates. The corresponding figure and coefficients α_{i} are shown in the supplementary material.

It is interesting to compare the trends observed here with those reported by Attili et al. [10] for the hydrodynamic instability mechanism in methane/air flames. Attili et al. [10] reported an increase of cut-off wave numbers with increasing pressure, while for the present results at elevated temperature, a weak reduction of cut-off wave number with increasing pressure is observed. However, the same trends for the Zeldovich number and maximum growth rates (both increase with pressure) are seen in Attili et al. [10]. As pointed out by Attili et al. [10], the increase of Zeldovich numbers at higher pressures relates to a changing balance between the chain branching and chain termination reactions, which applies to methane/air as well as hydrogen/air flames, so the same trend is observed. Similarly for the other parametric variations, the cut-off wave length remains constant or reveals a weak increase towards unstable conditions, revealing an opposite trend of the cut-off wave length in thermodiffusively unstable flames compared to flames that are not affected by thermodiffusive instabilities.

One possible explanation, why the cut-off wave length λ_{c} is not increasing with pressure, is that λ_{c} is already close to the thermal flame thickness for the present cases in contrast to the methane/air flames of Attili et al. [10], so a significant further reduction of λ_{c} towards unstable conditions cannot be expected. For any fuel, even for the ones that are prone to thermodiffusive instabilities such as hydrogen, one would expected that the cut-off wave length λ_{c} is always larger or equal to a value that is in the order of the flame thickness $\lambda_{\mathrm{c}} \gtrsim l_{\mathrm{F}}$. For example for lean hydrogen flames, the differential diffusion of hydrogen, which leads to an accumulation of hydrogen in convex flame regions, can only lead to an instability if the variation of the hydrogen mass fraction along the flame front are sustained until the reaction layer is reached. However, if the scale of the perturbation is in the order of the flame thickness $\lambda \approx l_{\mathrm{F}}$, the spatial separation of the locations, where hydrogen is accumulated, is not large enough compared to the thickness of the preheat zone such that the hydrogen fluctuations are equalized by diffusion within the preheat zone before the reaction layer is reached and no instability is seen.

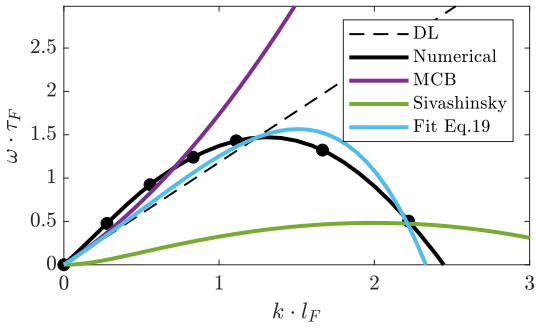

(a) Case 'Ref'

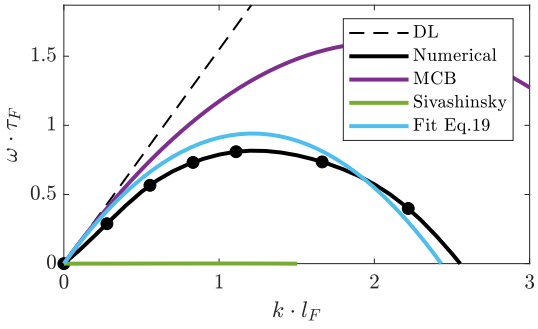

(b) Case 'Eq100'

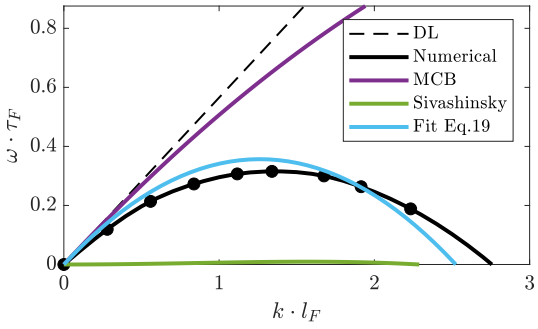

(c) Case 'Tu700'

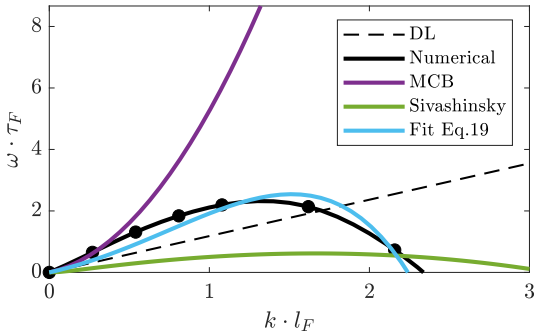

(d) Case 'p10'

Figure 9: Comparison of numerical dispersion relations and different theoretical models: Symbols refer to growth rates obtained from simulations, solid black lines represent cubic spline fits to the simulation data, and dashed lines are the growth rates associated with the hydrodynamic instability. Theoretical models: Eq. 1 by Matalon et al. [14] (purple solid lines labeled *MCB*), Eq. 10 by Sivashinsky [9] (green solid lines), and Eq. 19 that fits a polynomial to the numerical data (blue solid lines labeled *Fit*). For each case, growth rates and wave numbers are normalized by the flame time τ_F and flame thickness l_F.

4.3. Comparison with Theoretical Models

Fig. 9 shows a comparison of the theoretical models and numerical dispersion relations for selected cases. The comparison of all cases can be found in the supplementary material. For the cases 'Ref' and 'p10', the model by Matalon et al. [14] predicts an indefinite increase of growth rates for large wave numbers as the second order term has a positive contribution due to the low effective Lewis number and large Zeldovich number. As this model does not contain terms of order larger than two in its series expansion, it is expected that it cannot capture the flame stabilization at large wave numbers. For the cases 'Eq100' and 'Tu700', a stabilization at large wave numbers is predicted as the second order term has a negative contribution, but the decline of growth rates towards large wave numbers is significantly smaller compared to the numerical dispersion relations. However, the trends of the model by Matalon et al. [14] are qualitatively in agreement with the findings obtained from the power law fit of Eq. 17, where an increase of σ and β increases growth rates while an increase of Le_{eff} decreases growth rates. It is worth noting that the model of Matalon et al. [14] can also reproduce the changing nature of the thermodiffusive mechanism from a stabilizing to a destabilizing mechanism if β is increased. For example, for case 'Tu700', the numerical growth rates and the model prediction are always below the ones associated with the hydrodynamic instability at any wave number in Fig. 9c indicating that the contribution of the thermodiffusive mechanism is negative. However, when the Zeldovich number increases due to the increase of pressure, numerical growth rates and model predictions that exceed the growth rates of the hydrodynamic instability are visible, e.g. for case 'Tu700p20' (cf. supplementary material), indicating that the themodiffusive mechanism acts destabilizing at intermediate values of the wave number.

The model by Sivashinsky [9] significantly underpredicts growth rates for all cases as it neglects the effect of density variation throughout the flame front, which is particularly relevant for the contribution of the hydrodynamic instability mechanism. However, consistent with the power law fit of Eq. 17, it is found to also predict an increase of growth rates if β is increased or if Le_{eff} is decreased.

To assess whether an extension of the model by Matalon et al. [14] by a fourth order term, as suggested in Eq. 14 and similar to Yuan et al. [16], could improve predictions, the following dispersion relation is analyzed

$$\overline{\omega} = \omega_{\text{DL}} \cdot \overline{k} + \Pi_{k^2,\text{Fit}} \cdot \overline{k}^2 - \Pi_{k^4,\text{Fit}} \cdot \overline{k}^4, \tag{19}$$

where the coefficients $\Pi_{k^2,\text{Fit}}$ and $\Pi_{k^4,\text{Fit}}$ are fitted to the numerical dispersion relations for each case. It is worth noting that $\Pi_{k^4,\text{Fit}}$ is constrained to be positive while the value of $\Pi_{k^2,\text{Fit}}$ is unconstrained. In Fig. 9, the least unstable cases 'Eq100' and 'Tu700' are reasonably well approximated by Eq. 19 while for the strongly unstable cases 'Ref' and 'p10', qualitatively different shapes are obtained for the fits compared to the numerical values. Particularly towards small wave numbers, the fit underpredicts growth rates and the peak growth rate is located at different wave numbers. To match the numerical growth rates of

Table 2: Comparison of the second order term $\Pi_{k^2,\mathrm{MCB}}$ in the model of Matalon et al. [14] with the model of Eq. 19 that fits a second and fourth order term, $\Pi_{k^2,\mathrm{Fit}}$ and $\Pi_{k^4,\mathrm{Fit}}$, to the numerical dispersion relations.

Case name	$\Pi_{k^2,\mathrm{MCB}}$	$\Pi_{k^2,\mathrm{Fit}}$	$\Pi_{k^4,\mathrm{Fit}}$
Ref	0.55	0.30	0.17
Eq040	1.62	0.66	0.25
Eq065	-0.03	-0.16	0.08
Eq100	-0.37	-0.66	$< 10^{-6}$
Tu500	0.06	0.01	0.06
Tu700	-0.06	-0.23	$< 10^{-6}$
p05	2.08	0.85	0.29
p10	4.07	1.15	0.36
Tu700p03	0.01	-0.05	0.03
Tu700p10	0.31	0.19	0.10
Tu700p20	0.73	0.44	0.20

the unstable cases 'Ref' and 'p10' with the fit of Eq. 19 at small wave numbers, a large positive value of $\Pi_{k^2,\mathrm{Fit}}$ would be required. However, this would induce very large discrepancies at large wave numbers that cannot be adequately compensated by the fourth order term. This suggests that for the unstable cases 'Ref' and 'p10', higher order terms of the expansion series of the wave number $\bar{k}$ are missing in Eq. 19 or in other words, a series expansion in $\bar{k}$ may not be an adequate description of the dispersion relation while the dispersion relations of the stable cases 'Eq100' and 'Tu700' appear to be well described by a low-order polynomial function. In general, a good agreement of Eq. 19 and the numerical dispersion relations is only obtained for cases 'Eq100' and 'Tu700', while for all other cases, qualitative differences with respect to the shape of the curves are visible.

Furthermore, Tab. 2 compares the values of $\Pi_{k^2,\mathrm{Fit}}$ with the corresponding term in the model by Matalon et al. [14]. The coefficient $\Pi_{k^2,\mathrm{MCB}}$ in the model is defined as

$$\Pi_{k^2,\mathrm{MCB}} = -\delta[B_1 + \beta(Le_{\mathrm{eff}} - 1)B_2 + PrB_3]. \tag{20}$$

From Tab. 2, it becomes evident that $\Pi_{k^2,\mathrm{Fit}} < \Pi_{k^2,\mathrm{MCB}}$ for all cases. The fitted values $\Pi_{k^2,\mathrm{Fit}}$ may change if fitting higher order polynomials to the numerical dispersion relations as the numerical and fitted dispersion relations possess different shapes, but for the less unstable cases 'Eq100' and 'Tu700', the fits are in good agreement with the numerical dispersion relations indicating that these cases can be well represented by a second-order polynomial function (note that $\Pi_{k^4,\mathrm{Fit}} < 10^{-6}$). Thus, the deficiencies of the model by Matalon et al. [14] for these cases are most likely not related to the negligence of higher order terms in Eq. 1, but possibly arise from the effective Lewis numbers of these cases that are not close to unity in contrast to the model assumption.

5. Conclusion

A series of detailed numerical simulations of lean premixed hydrogen flames with varying equivalence ratio, unburned temperature, and pressure has been performed to extract numerical dispersion relations at different conditions. In this stability analysis, the growth rates of weak harmonic perturbations of the flame front were measured with respect to the wave length of the perturbation. This allowed for a rigorous analysis of the contributions of the different intrinsic instability mechanisms such as the hydrodynamic and thermodiffusive instability.

A decrease of equivalence ratio and unburned temperature and an increase of pressure have been found to enhance growth rates in the dispersion relation and, hence, intrinsic instabilities. In particular, the propensity of intrinsic instabilities to increase with rising pressure is relevant to several combustion devices that operate at elevated pressures. Growth rates have been found to be increased if either the expansion ratio or the Zeldovich number are increased or if the effective Lewis number of the mixture is decreased. The numerical dispersion relations have been compared to various theoretical models, but none can quantitatively predict the numerical dispersion relations at any conditions. However, trends with respect to the expansion ratio, the Zeldovich number, and the effective Lewis number are qualitatively correctly captured. Furthermore, a polynomial whose form has been adopted from theoretical models has been fitted to the dispersion relations. Cases, in which the thermodiffusive mechanism is stabilizing, have been found to be well represented by a second-order polynomial function while cases, in which the thermodiffusive mechanism is destabilizing, could not be matched by a fourth-order polynomial function indicating that several higher-oder terms are required for an accurate prediction.

The analysis of strongly corrugated flame fronts in the nonlinear phase of the flame evolution is pursued in the second part of this work [22].

Acknowledgment

Generous support of the Deutsche Forschungsgemeinschaft (DFG) under grant number PI 368/9-1 is gratefully acknowledged. Computational resources have been provided by the Gauss Centre for Supercomputing e.V. on the GCS Supercomputer SuperMuc at Leibniz Supercomputing Centre in Munich.

References

[1] J. Perner, D. Bothe, Report for the World Energy Council German by Frontier Economics Ltd. (2018).
[2] A. Sartbaeva, V.L. Kuznetsov, S.A. Wells, P.P. Edwards, Hydrogen nexus in a sustainable energy future, Energ. Environ. Sci. 1 (2008) 79–85.
[3] S. Verhelst, T. Wallner, Hydrogen-fueled internal combustion engines, Prog. Energ. Combust. 35 (2009) 490–527.
[4] P. Clavin, F.A. Williams, Effects of molecular diffusion and of thermal expansion on the structure and dynamics of premixed flames in turbulent flows of large scale and low intensity, J. Fluid Mech. 116 (1982) 251–282.
[5] M. Matalon, B.J. Matkowsky, Flames of gasdynamics discontinuities, J. Fluid Mech. 124 (1982) 239–259.

[6] G.K. Giannakopoulos, A. Gatzoulis, C.E. Frouzakis, M. Matalon, A.G. Tomboulides, Consistent definitions of "flame displacement speed" and "Markstein length" of premixed flame propagation, Combust. Flame 162 (2015) 1249–1264.

[7] P. Clavin, J.C. Graña-Otero, Curved and stretched flames: the two Markstein numbers, J. Fluid Mech. 686 (2011) 187–217.

[8] G.I. Sivashinsky, Diffusional-Thermal Theory of Cellular Flames, Combust. Sci. Technol. 15 (1977) 137–146.

[9] G.I. Sivashinsky, Nonlinear analysis of hydrodynamic instability in laminar flames - I. Derivation of basic equations, Acta Astronaut. 4 (1977) 1177–1206.

[10] A. Attili, R. Lamioni, L. Berger, K. Kleinheinz, P.E. Lapenna, H. Pitsch, F. Creta, The effect of pressure on the hydrodynamic stability limit of premixed flames, Proc. Comb. Inst. 38 (2021) 1973–1981.

[11] L. Berger, K. Kleinheinz, A. Attili, H. Pitsch, Characteristic patterns of thermodiffusively unstable premixed lean hydrogen flames, Proc. Comb. Inst. 37 (2019) 1879–1886.

[12] C.E. Frouzakis, N. Fogla, A.G. Tomboulides, C. Altantzis, M. Matalon, Numerical study of unstable hydrogen/air flames: Shape and propagation speed, Proc. Combust. Inst. 35 (2015) 1087–1095.

[13] C. Altantzis, C. E. Frouzakis, A. G. Tomboulides, M. Matalon, K. Boulouchos, Hydrodynamic and thermodiffusive instability effects on the evolution of laminar planar lean premixed hydrogen flames, J. Fluid Mech. 700 (2012) 329–361.

[14] M. Matalon, C. Cui, J. K. Bechtold, Hydrodynamic theory of premixed flames: effects of stoichiometry, variable transport coefficients and arbitrary reaction orders, J. Fluid Mech. 487 (2003) 197–210.

[15] S. Kadowaki, T. Hasegawa, Numerical simulation of dynamics of premixed flames: flame instability and vortex–flame interaction, Prog. Energ. Combust. 31 (2005) 193–241.

[16] J. Yuan, Y. Ju, C. K. Law, On flame-front instability at elevated pressures, Proc. Comb. Inst. 31 (2007) 1267–1274.

[17] G.J. Sharpe, Linear stability of planar premixed flames: reactive Navier–Stokes equations with finite activation energy and arbitrary Lewis number, Combust. Theor. Model. 7 (2003) 45–65.

[18] B. Denet, P. Haldewang, A Numerical Study of Premixed Flames Darrieus-Landau Instability, Combust. Sci. Technol. 104 (1995) 143–167.

[19] Z. Zhou, F.E. Hernandez-Perez, Y. Shoshin, J.A. van Oijen, L.P.H. de Goey, Effect of Soret diffusion on lean hydrogen/air flames at normal and elevated pressure and temperature, Combust. Theor. Model. 21 (2017) 879–896.

[20] J. Schlup, G. Blanquart, Validation of a mixture-averaged thermal diffusion model for premixed lean hydrogen flames, Combust. Theor. Model. 22 (2018) 264–290.

[21] H. Boughanem, A. Trouvé, The domain of influence of flame instabilities in turbulent premixed combustion, Proc. Comb. Inst. 27 (1998) 971–978.

[22] L. Berger, A. Attili, H. Pitsch, Enhancement of Intrinsic Instabilities in Premixed Hydrogen Flames due to Variations of Pressure, Equivalence Ratio, and Temperature: Part 2 - Flame Speed and Flame State of Strongly Corrugated Flames, Combust. Flame (2021).

[23] N. Peters, F.A. Williams, The Asymptotic Structure of Stoichiometric Methane-Air Flames, Combust. Flame 68 (1987) 185–207.

[24] C.J. Sun, C.J. Sung, L. He, C.K. Law, Dynamics of Weakly Stretched Flames: Quantitative Description and Extraction of Global Flame Parameters, Combust. Flame 118 (1999) 108–128.

[25] G. Joulin, T. Mitani, Linear stability analysis of two-reactant flames, Combust. Flame 40 (1981) 235–246.

[26] L. Landau, On the theory of slow combustion., Acta Physicochim. URS. 19 (1944).

[27] G. Darrieus, Propagation d'un front de flamme, 1945. Presented at Le congres de Mecanique Appliquee (unpublished).

[28] G.I. Sivashinsky, Instabilities, pattern formation, and turbulence in flames, Ann. Rev. Fluid Mech. 15 (1983) 179–199.

[29] H. Pitsch, A C++ program package for 0D combustion and 1D laminar flames, 1998.

[30] P. Chiesa, G. Lozza, L. Mazzocchi, Using hydrogen as gas turbine fuel, J. Eng. Gas Turb. Power 127 (2005) 73–80.

[31] A. Tomboulides, J. Lee, S. Orszag, Numerical simulation of low Mach number reactive flows, J. Scientif. Comput. 12 (1997) 139–167.

[32] M.P. Burke, M. Chaos, Y. Ju, F.L. Dryer, S.J. Klippenstein, Comprehensive H_2/O_2 kinetic model for high-pressure combustion, Int. J. Chem. Kinet. 44 (2012) 444–474.

[33] C.R. Wilke, A Viscosity Equation for Gas Mixtures, J. Chem. Phys. 18 (1950) 517–519.

[34] R.B. Bird, W.E. Stewart, E.N. Lightfoot, Transport Phenomena, John Wiley & Sons, Inc., 2007.

[35] A. Eucken, Über das Wärmeleitvermögen,die spezifische Wärme und die innere Reibung der Gase, Physik. Z. 14 (1913).

[36] S. Mathur, P. Tondon, S. Saxena, Thermal conductivity of binary, ternary and quaternary mixtures of rare gases, Mol. Phys. 12 (1967) 569–579.

[37] J. Schlup, G. Blanquart, A reduced thermal diffusion model for H and H_2, Combust. Flame 191 (2018) 1–8.

[38] A. Attili, F. Bisetti, M.E. Mueller, H. Pitsch, Effects of non-unity Lewis number of gas-phase species in turbulent nonpremixed sooting flames, Combust. Flame 166 (2016) 192–202.

[39] O. Desjardins, G. Blanquart, G. Balarac, H. Pitsch, High order conservative finite difference scheme of variable density low Mach number turbulent flows, J. Comput. Phys. 227 (2008) 7125–7159.

[40] R.D. Falgout, U.M. Yang, hypre: A library of high performance preconditioners, in: Computational Science—ICCS 2002, Springer, 2002, pp. 632–641.

[41] G.S. Jiang, C.W. Shu, Efficient implementation of weighted ENO schemes, J. Comput. Phys. 126 (1996) 202–228.

[42] G. Strang, On the construction and comparison of difference schemes, SIAM J. Numer. Anal. 5 (1968) 506–517.

[43] A.C. Hindmarsh, P.N. Brown, N. Peter, K.E. Grant, S.L. Lee, R. Serban, D.E. Shumaker, C.S. Woodward, SUNDIALS: Suite of nonlinear and differential/algebraic equation solvers, ACM T. Math. Software 31 (2005) 363–396.

[44] J. Beeckmann, R. Hesse, S. Kruse, A. Berens, N. Peters, H. Pitsch, M. Matalon, Propagation speed and stability of spherically expanding hydrogen/air flames: Experimental study and asymptotics, Proc. Comb. Inst. 36 (2017) 1531–1538.

[45] Y. Wang, A. Movaghar, Z. Wang, Z. Liu, W. Sun, F.N. Egolfopoulos, Z. Chen, Laminar flame speeds of methane/air mixtures at engine conditions: Performance of different kinetic models and power-law correlations, Combust. Flame 218 (2020) 101–108.